Articles

Characterization of $[4Fe\text{-}4Se]^{2+/3+}$ High-Potential Iron–Sulfur Protein from *Chromatium vinosum*

Jean-Marc Moulis,*,‡ Marc Lutz,§ Jacques Gaillard,∥ and Louis Noodleman∥

DRF-LBio-Biochimie Microbienne and DRF-SPh-SCPM, CENG 85X, 38041 Grenoble Cedex, France, and DB-Biophysique, CEN-Saclay, 91191 Gif-sur-Yvette Cedex, France

Received March 14, 1988; Revised Manuscript Received June 14, 1988

ABSTRACT: Selenium atoms have been introduced into *Chromatium vinosum* high-potential iron–sulfur protein (HiPIP) in place of inorganic sulfur at the [4Fe-4S] active site. The substitution induces a decrease of the redox potential by ca. 65 mV (from 350 to 285 mV vs NHE, 25 °C, pH 7.8) and results in changes of the optical and EPR spectra. Compared to the corresponding properties of native HiPIP, some of the charge-transfer transitions of the Se derivative shift to lower energies, and the almost axial $S = {}^1/_2$ EPR signal occurs at lower field with a larger anisotropy. As in the case of clostridial ferredoxins, the resonance Raman spectra of reduced HiPIP are very sensitive to S*/Se substitution. The bridging stretching modes of the inorganic core shift to lower frequencies upon replacement of S* by Se as expected, but the local D_{2d} symmetry assumed by the active site remains. The availability of the Se derivative has further allowed us to define the vibrational properties of the oxidized cluster. The bridging modes are only marginally affected by electron removal, and thus, the relevant symmetry point group for the inorganic core is the same as at the reduced level (D_{2d}). In contrast, the Fe–Scys stretching modes occur at higher frequencies with larger splittings, implying that the major effect of oxidation is to strengthen and distort the Fe–Scys bonds. These data strongly suggest that one or two of the latter bonds play a crucial role in the electron exchange reaction between the active site and the redox partners of HiPIP.

High-potential iron–sulfur proteins (HiPIP)[1] have been mainly isolated from purple sulfur bacteria (Bartsch, 1978). Their active site is organized around a [4Fe-4S] cluster, structurally almost identical (Carter, 1977) with those of the well-known ferredoxins (Fd). However, all HiPIPs characterized to date display positive redox potentials (Mizrahi et al., 1980), in striking contrast with those of Fd, usually found around −400 mV relative to the normal hydrogen electrode (NHE). The discrepancy has been explained by the so-called "three states hypothesis" (Carter et al., 1972), according to which the $[Fe_4S_4Scys_4]^{-/2-}$ redox transition is operative in HiPIP instead of the 2−/3− one in Fd. According to X-ray crystallographic results (Carter et al., 1974), the molecular basis for the use by HiPIP of a redox transition involving less charged forms of the cluster has been assigned to a more hydrophobic environment of the active site than in Fd; this feature correlates with a lower number of charge-stabilizing hydrogen bonds to the inorganic complex in HiPIP (Carter, 1977). Despite the abundant structural and spectroscopic data, including resonance Raman (RR) spectra (Spiro et al., 1982; Johnson et al., 1983), available for these proteins, their exact physiological function is still largely undefined.

The substitution of inorganic sulfur by selenium in tetranuclear clusters has been used to assess the precise role played by the chalcogenide atoms in this complex structure (Bobrik et al., 1978; Meyer & Moulis, 1981). The overall properties of *Clostridium pasteurianum* Fd are not drastically affected by chalcogenide replacement (Moulis & Meyer, 1982), but all reduced selenium-containing clostridial Fd examined to date display unusual EPR and Mössbauer features which have been attributed to the occurrence of high-spin ground states (Moulis et al., 1984a; Gaillard et al., 1986). Some of these properties (Auric et al., 1987) surprisingly mimic those observed with more complex proteins such as the nitrogenase Fe-protein (Lindahl et al., 1985). Moreover, Se can be used as a very efficient vibrational probe in iron–sulfur clusters (Meyer et al., 1986a,c; Moulis et al., 1984b).

Changes induced by selenium in HiPIP have been studied here with the protein isolated from *Chromatium vinosum* (Chv). The possibility of replacing inorganic sulfur by selenium in this class of proteins is demonstrated, and the properties of the substituted material are described. RR spectra are reported for both redox levels reached in HiPIP, and the presence of Se at the active site helps in assigning the vibrational modes. These data give insight into the reorganization occurring upon electron transfer.

Materials and Methods

C. vinosum HiPIP was a kind gift from Dr. M. A. Cusanovich (University of Arizona, Tucson). This material was further loaded on a DEAE-cellulose column (DE-52, Whatman, U.K.) equilibrated in 10 mM Tris-HCl, pH 8.0, and developed with a linear NaCl gradient (0–0.2 M) in the same buffer. After concentration on a Amicon YM 5 membrane, the HiPIP solution was filtrated through Sephadex G-50

‡ DRF-LBio-Biochimie Microbienne, CENG.
§ DB-Biophysique, CEN-Saclay.
∥ DRF-SPh-SCPM, CENG.

[1] Abbreviations: HiPIP, high-potential iron–sulfur protein; Fd, ferredoxin; NHE, normal hydrogen electrode; Cp, *Clostridium pasteurianum*; Chv, *Chromatium vinosum*; DTT, dithiothreitol; X, sulfur or selenium; EPR, electron paramagnetic resonance; RR, resonance Raman; IR, infrared; ENDOR, electron–nuclear double resonance; HOMO, highest occupied molecular orbital; LUMO, lowest unoccupied molecular orbital.

0006-2960/88/0427-8712$01.50/0

(Pharmacia) equilibrated in 50 mM Tris-HCl containing 0.1 M NaCl, pH 8, and the final protein solution displayed a purity index A_{283}/A_{388} of less than 2.5, indicative of homogeneous material (Bartsch, 1978; vide infra).

Electronic spectra were recorded with a Cary 219 spectrophotometer (Meyer & Moulis, 1981) and EPR spectra with a Varian E-109 spectrometer (Moulis et al., 1984a) as already described. The method used to obtain low-temperature resonance Raman spectra has been presented elsewhere (Lutz, 1977; Lutz et al., 1983).

Iron was assayed by bathophenanthrolinedisulfonate chelation (Blair & Diehl, 1961) after mineralization.

Midpoint redox potentials were determined by potentiometric titration with the ferrocyanide–ferricyanide redox couple as oxidative titrant, the extent of oxidation being followed by the development of the EPR signal. The potentiometric cell was installed inside a glovebox (Jacomex, Livry Gargan, France) ensuring an oxygen atmosphere of less than 1.5 ppm and was operated with a saturated calomel electrode as reference and a platinum grid as working electrodes. Other experimental conditions are given in the legend of Figure 4.

ApoHiPIP Preparation. The inorganic cluster of HiPIP was removed, under strictly anaerobic conditions, by the following method. A protein solution, initially about 25 mg/mL in 50 mM Tris-HCl containing 0.1 M NaCl, pH 8, was diluted with distilled water to a concentration of about 1 mg/mL, and guanidine hydrochloride was added to a final concentration of 5 M. The medium was cooled to 4 °C, and 12 N HCl was added to a final concentration of 0.5 N: the brown solution immediately turned pink and rapidly (in about 1 min) became colorless. The resulting clear solution was agitated under Ar flow for 30 min and then neutralized with a concentrated Tris–base solution to pH 7. The apoprotein thus obtained was dialyzed overnight in Spectra-Por 3 tubing treated with a sulfide-removing solution (Spectrum) versus 2.5 L of 5 mM Tris-HCl, pH 7.8, with two buffer changes. The protein solution was subsequently precipitated with 8% trichloroacetic acid for 30 min under Ar and recovered by centrifugation. The white protein pellet was rinsed with distilled water and resuspended in a minimal volume of 0.5 M Tris-HCl, pH 8.5. The solution was finally filtrated on a 5-mL Sephadex G-10 column equilibrated in 50 mM Tris containing 0.1 M NaCl, pH 7.7; the protein recovery was about 100% at this stage. The resulting material had no significant absorbance above 350 nm (Figure 1) and gave the best results in the reaction of reinsertion of inorganic elements.

Iron and Selenium Incorporation into ApoHiPIP. ApoHiPIP was reacted with $FeCl_3$ and a mixture of Na_2SeO_3 and excess DTT as previously described for Fd (Moulis & Meyer, 1982). The only modification was the increase of the ionic strength of the medium (0.25 M Tris-HCl, 0.2 M NaCl, pH 7.7) which obliged dilution of the solution by 10 volumes of distilled water prior to loading of the DE-52 column. When a 16-fold molar excess of reactants over HiPIP was used, the protein containing selenium was recovered with 40% yield.

Results

The procedures previously described to remove the inorganic elements from Fd (Moulis & Meyer, 1982; Meyer et al., 1986b) failed to provide the HiPIP molecule perfectly devoid of iron and sulfur. Complete removal of the iron–sulfur cluster from HiPIP required all the participants of the reaction to be kept in solution; this has been achieved by first destroying the inorganic core with 0.5 M HCl and then removing the low molecular weight components by dialysis after neutralization (Materials and Methods). The very low residual absorbance

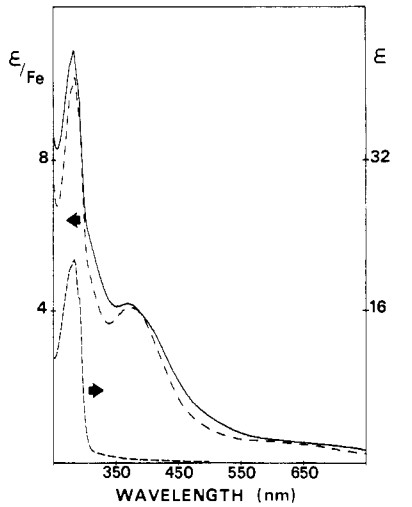

FIGURE 1: UV–visible absorption spectra of reduced Chv HiPIP: (lower spectrum) apoHiPIP; (—) [4Fe-4Se]$^{2+}$ HiPIP; (--) [4Fe-4S]$^{2+}$ HiPIP. All spectra were recorded in 50 mM Tris-HCl containing 0.1 M NaCl, pH 7.8. ϵ is the extinction coefficient in mM^{-1} cm^{-1}.

in the visible part of the spectrum of Figure 1 (lower trace) clearly indicates that no chromophoric complex remains bound to apoHiPIP in these conditions. Additional data on Se-reconstituted material (see below) confirm the absence of inorganic elements in the apoprotein preparations.

By contrast, no important change in the conditions used to refold Cp Fd around [4Fe-4Se] clusters (Moulis & Meyer, 1982) has been necessary to perform the same reaction with apoHiPIP. However, an increase in the ionic strength of the reaction medium (up to 0.2 M NaCl, 0.25 M Tris) did improve the yield. These features of both apoHiPIP preparation and Se incorporation are in agreement with the well-known higher stability of HiPIP proteins as compared to that of Fd: a rationale for this property is given by crystallographic results which show the Fe–S cluster as more buried inside the relatively large HiPIP (Carter et al., 1974) than in smaller Fd where the active sites display good accessibility to the solvent (Adman et al., 1973).

As already reported (Bartsch, 1971), the visible absorption spectrum of reduced native HiPIP (Figure 1) is very similar to those of oxidized Fd (Meyer & Moulis, 1981). The Se analogue of Cp Fd displays a spectrum with a broad visible envelope reminiscent of that of native Fd except for a slightly higher absorption coefficient over the whole wavelength range (Meyer & Moulis, 1981). Figure 1 shows that S/Se substitution in HiPIP induces almost exactly the same spectral changes, except for a shoulder appearing at ca. 425 nm. The hypsochromic shift of the lower energy maximum upon chalcogenide replacement is the same (388 → 386 nm) as observed with ferredoxins (Meyer & Moulis, 1981).

Ferricyanide-oxidized HiPIP has an almost featureless absorption spectrum, rising in intensity toward short wavelengths, with very weak absorbance variations between 360 and 450 nm (Bartsch, 1971; Figure 2). The spectrum of Se-substituted HiPIP follows the same pattern except that a broad band forming a shoulder at ca. 450 nm occurs at lower energy (Figure 2). The latter feature seems to be the counterpart of a ca. 440-nm band revealed at 9 K in the spectrum of native HiPIP (Johnson et al., 1981). The absorbance of both native and Se-substituted HiPIP in the visible range increases upon oxidation (Figures 1 and 2).

The X-band EPR spectrum of oxidized HiPIP is dominated by an axial signal with $g_{\parallel} = 2.12$ and $g_{\perp} = 2.04$ (Figure 3) attributed to a $S = {}^1/_2$ ground spin state (Antanaitis & Moss, 1975). In addition, weaker features occur at apparent g values

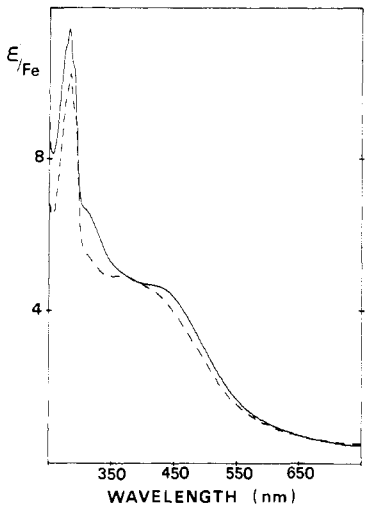

FIGURE 2: UV–visible absorption spectra of oxidized Chv HiPIP: (—) $[4Fe\text{-}4Se]^{3+}$ HiPIP; (– –) $[4Fe\text{-}4S]^{3+}$ HiPIP. Ferri(ferro)cyanide was removed from the samples by passage through a 0.5-mL Dowex AG 1X8 column. Other conditions as in Figure 1.

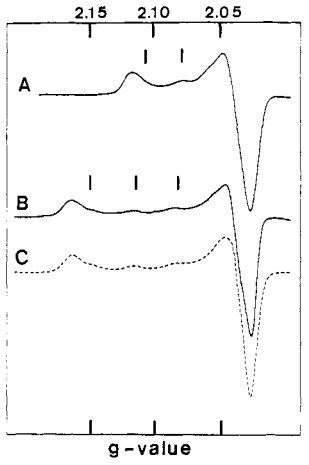

FIGURE 3: EPR spectra of Chv HiPIP. (A) Native HiPIP. (B) Se-substituted HiPIP. Both spectra were recorded at 12 K in 50 mM Tris-HCl containing 0.1 M NaCl, pH 7.8. Vertical bars denote minor components referred to in the text. Instrument settings: microwave power, 1 mW; modulation amplitude, 0.8 mT; field modulation, 100 kHz; klystron frequency, 9.224 GHz. (C) Simulation of the spectrum in (B), assuming four tensors of main g values (2.168, 2.034, 2.028), (2.152, 2.038, 2.027), (2.117, 2.044, 2.035), and (2.085, 2.048, 2.035) with respective weights of 65, 18, 10, and 7%.

of 2.108, 2.08, and 2.055 (Figure 3). The EPR spectral pattern associated with oxidized HiPIP varies widely from sample to sample; for instance, we have occasionally observed the splitting of the $g = 2.12$ absorption in two resolved peaks at $g = 2.124$ and $g = 2.117$. Also, the contribution of the $g = 2.08$ feature to the spectrum changes when compared to that of the 2.12 peak, even among samples prepared from the same protein solution. The major component of the upper spectrum of Figure 3 ($g_{\parallel} = 2.12$, $g_{\perp} = 2.04$) is more easily saturated by microwave power above 10 K than the signal associated with the $g = 2.08$ feature. The heterogeneity revealed by the EPR properties does not appear to result from a mixture of different proteins (isozymes for instance), since neither sodium dodecyl sulfate–polyacrylamide gel electrophoresis nor high-performance liquid chromatography under various conditions revealed the presence of more than one component in the protein preparations used in this work. The presence of overlapping EPR signals with Chv HiPIP is largely documented [see, for instance, Antanaitis and Moss (1975)] and has been attributed to a consequence of freezing the samples (Sands, 1979). The EPR spectrum of Se-substituted HiPIP

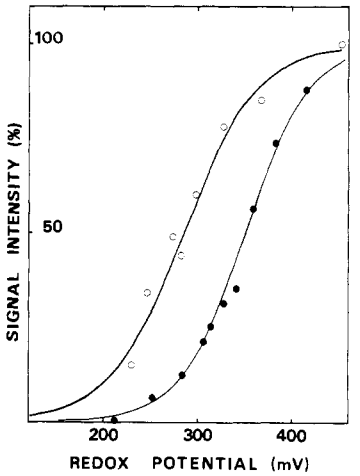

FIGURE 4: Midpoint redox potential of native and Se-substituted Chv HiPIP. (Open symbols) Se-substituted HiPIP; (closed symbols) native HiPIP. The ca. 0.1 mM reduced proteins in 50 mM Tris-HCl containing 0.1 M NaCl, pH 7.8, were titrated with small aliquots of a 10 mM ferricyanide solution in the same buffer. At each potential, 0.1-mL samples were withdrawn and immediately frozen in anaerobic EPR tubes for further analysis. EPR data were recorded as in Figure 2. The integrated signal was compared to the signal intensity obtained for the highest potential reached at the end of the titration. Other details are given under Materials and Methods. Curves are least-squares fits of the experimental data to the Nernst equation with $E_0 = +350$ mV and $E_0 = +285$ mV vs NHE for native and Se-substituted HiPIP, respectively.

is similar in many respects to that of native HiPIP: its main component ($g_1 = 2.168$, $g_2 = 2.034$, $g_3 = 2.028$) shows little departure from axiality (Figure 3) and displays a relative ease of saturation when compared to minor features at apparent g values of 2.152, 2.117, 2.085, and 2.055 (Figure 3). No other feature has been found below 0.3 T or above 0.33 T (not shown), in contrast with our findings with reduced Se-substituted clostridial Fd (Moulis et al., 1984a; Gaillard et al., 1986). Thus, except for a general shift of the EPR spectrum to lower fields (Figure 3), the electronic properties of oxidized Se-substituted HiPIP resemble closely those of the native protein, and the overlapping signals observed on the EPR spectra of both species (Figure 3) have most probably the same origin.

The development of the EPR signal has been used to monitor the extent of protein oxidation by ferricyanide during titration experiments. HiPIP containing either inorganic sulfur or selenium exchanges one electron with the oxidant. The midpoint redox potential has been determined by potentiometry at pH 7.8 during the course of the titration, and values of 350 ± 5 mV and 285 ± 12 mV vs NHE have been found for the native and Se-substituted proteins, respectively (Figure 4). The former value agrees with published data (Mizrahi et al., 1980).

The resonance Raman (RR) spectra of Figure 5 clearly show the different vibrational properties of native and Se-containing HiPIP. With 457.9-nm excitation, the $[4Fe\text{-}4S]^{2+}$ cluster exhibits RR spectra dominated by two bands at 342 and 364 cm^{-1} (Figure 5A), in qualitative agreement with previously published spectra (Spiro et al., 1982; Johnson et al., 1983; Czernuszewicz et al., 1987). The 364-cm^{-1} band involves two components, as indicated by its unsymmetrical shape and as confirmed by spectra excited at 496.5 nm (insert of Figure 5). At least six additional weaker lines occur in the 250–400-cm^{-1} range (Table I). The latter wavenumber region is characteristic for Fe–S stretching modes in iron–sulfur proteins (Spiro et al., 1982; Meyer et al., 1986a). The upper spectrum of Figure 5 is strikingly similar to those of Cp Fd

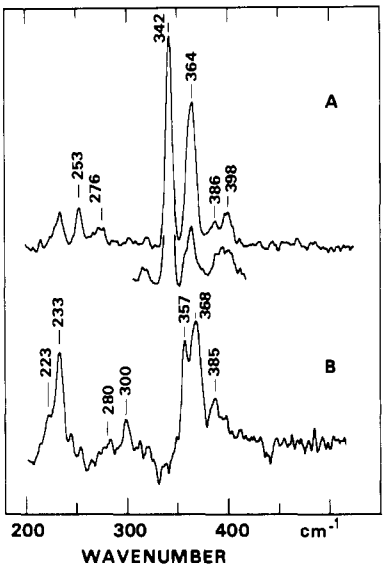

FIGURE 5: Low-temperature resonance Raman spectra of reduced Chv HiPIP. (A) Native Chv HiPIP in 50 mM Tris-HCl containing 0.1 M NaCl, pH 8; 11 scans. (B) Se-substituted Chv HiPIP in the same buffer, pH 7.7; 23 scans. The samples were frozen at ca. 25 K and the spectra recorded with a 457.9-nm excitation wavelength except for the insert of (A): 496.5 nm. Scanning speed, 50 cm^{-1}/min; slit width, 500 μm; time constant, 1.8 s.

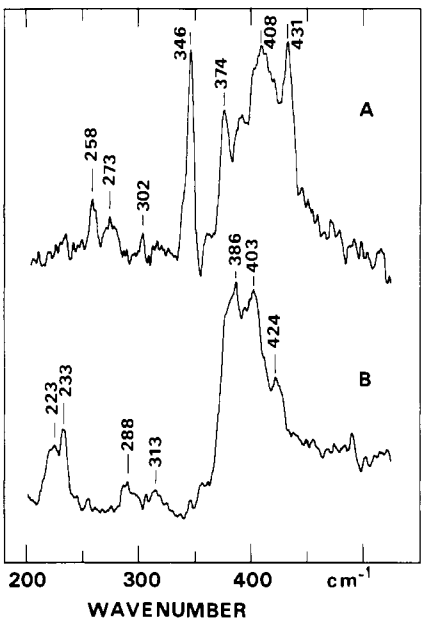

FIGURE 6: Low-temperature resonance Raman spectra of oxidized Chv HiPIP. (A) Native Chv HiPIP in 50 mM Tris-HCl, containing 0.2 M NaCl, pH 8; 10 scans. (B) Se-substituted Chv HiPIP in the same buffer, pH 7.7; 9 scans. Excitation wavelength: 496.5 nm. Other conditions as in Figure 5.

Table I: Resonance Raman Frequencies (cm^{-1}) of [4Fe-4X]$^{2+/3+}$ Clusters in Chv HiPIP[a]

[4Fe-4S]$^{2+}$	[4Fe-4S]$^{3+}$	[4Fe-4Se]$^{2+}$	[4Fe-4Se]$^{3+}$
234[b]	258 m	223 sh	223 m
253 m	273[c]	233 m[b]	233 s[b]
276[c]	302 vw	246[d]	288[c]
301 vw	346 s	255[d]	313 w
319 vw[b]	360 w	280[c]	357 w
342 s	374 s	300 w	376 sh
360 sh	389 s	320[b,d]	386 s
364 s	401 sh	357 s	394[d]
386 w	408 s	368 s	403 s
398 w	418 sh	385 m	412 sh[d]
	431 s	397 vw[d]	424 m

[a] Experimental conditions as in Figures 5 and 6. The correspondences of wavenumbers in a row do not imply the assignments of the bands to the same vibrational mode (see text for a discussion on assignments). Abbreviations: s, strong; m, medium; w, weak; sh, shoulder; v, very. [b] Band which may arise, at least in part, from the Raman scattering of ice (Meyer et al., 1986c). [c] Broad feature which may contain more than one band. [d] Extremely weak band, the existence of which is doubtful.

(Moulis et al., 1984b,c; Czernuszewicz et al., 1987); the only significant difference lies in the apparently smaller splitting, in the case of HiPIP, between the ca. 360-cm^{-1} modes attributed to Fe–Scys stretchings (Moulis et al., 1984c). A similar trend is displayed by *Bacillus stearothermophilus* Fd, the RR spectra of which have only one unresolved band at 360 cm^{-1} (Lutz et al., 1983), and such a feature cannot therefore be considered as characteristic of HiPIP. The Raman-active modes of [4Fe-4Se]$^{2+}$ HiPIP (Figure 5B) occur in roughly the same wavenumber range as those of the native protein but with a completely different distribution (Table I). The spectrum of the selenium derivative is also very similar to the one observed with 2[4Fe-4Se] Cp Fd (Moulis et al., 1984b). Analysis of the latter has shown that most of the cluster modes are shifted to lower frequencies upon S/Se substitution, as expected from the replacement of an atom by a much heavier one (Moulis et al., 1984c). At ca. 230 cm^{-1}, the presence of a large proportion of the signal corresponding to the Raman scattering of ice is excluded here since, at a given excitation wavelength, the ratio of the intensities of the 233- and 368-cm^{-1} lines is constant for a range of samples with different protein concentrations. Moreover, the main component of the ice spectrum (Meyer et al., 1986c) does not display any structure, in contrast with the features exhibited between 220 and 230 cm^{-1} in Figures 5 and 6. Last, the exchange of a sample of oxidized Se-HiPIP against D_2O failed to alter the spectral pattern, apart from slight shifts to lower frequencies (not shown). Thus, the main difference between the RR spectra of Fd (Moulis et al., 1984b) and HiPIP (Figure 5) containing Se is the presence in the latter spectrum of a set of bands at 385–397 cm^{-1}, in a spectral region dominated by Fe–Scys stretching modes (Moulis et al., 1984c).

RR spectra of ferricyanide-oxidized HiPIP are shown in Figure 6. They were obtained with 496.5-nm excitation, a wavelength lying on the low-energy side of the main visible bands of the absorption spectra (Figure 2). This wavelength has been found to be the most efficient, in the 351.1–496.5-nm range, in enhancing the vibrational Raman modes of the active site. Compared to those of the spectra of [4Fe-4X]$^{2+}$ clusters (Figure 5), the Raman-active modes of the oxidized species span a similar wavenumber range, but they extend to higher (up to ca. 435 cm^{-1}) frequencies (Figure 6). Also, the modes occurring between 370 and 435 cm^{-1} receive higher resonance enhancements than those found at lower frequencies: as a result, the spectra are dominated by a broad set of at least four, and probably six, bands between 370 and 435 cm^{-1} (Table I). Outside this frequency range, the Raman patterns displayed by the oxidized and reduced proteins are very similar: all the bands in the RR spectra of oxidized HiPIP (Figure 6) are shifted to slightly higher frequencies (usually by less than 10 cm^{-1}) when compared to the closest corresponding bands (below 350 cm^{-1}) in spectra of reduced proteins (Figure 5). For instance, the strong 346-cm^{-1} band in the spectrum of oxidized native HiPIP (Figure 6A) is clearly reminiscent of the 342 cm^{-1} one observed with the reduced protein (Figure 5A). Thus, on the basis of the assignments provided for ferredoxins (Moulis et al., 1984c; Czernuszewicz et al., 1987) and apparently relevant for reduced HiPIP (see Discussion),

the bands observed below 350 cm^{-1} in the spectra of Figure 6 most probably arise from Fe–X* stretching modes. Also, the presence of a similar group of bands in the spectra of both native and Se-substituted oxidized HiPIP between 370 and 435 cm^{-1} (Figure 6) leads to their assignment mainly to Fe–Scys stretchings, their higher apparent number in the case of native protein being probably due to the overlap of bridging modes in this region, as noticed at other redox levels (see above; Moulis et al., 1984c; Czernuszewicz et al., 1987). Although detailed assignments of the vibrational modes cannot be attempted with the present data, comparison of the RR spectra of both native and Se-substituted HiPIP indicates the occurrence of terminal modes in roughly the same frequency range but that of bridging modes for Se-HiPIP at lower wavenumbers than for S-HiPIP, as expected and already observed with ferredoxins (Moulis et al., 1984c).

Discussion

The present work was aimed at substituting the inorganic sulfur atoms of the active site of Chv HiPIP with selenium to examine the role played by the core chalcogenide in the structure and properties of high-potential tetranuclear clusters. Since Se^{2-} has a slightly larger ionic radius than S^{2-} (+6–10%), its involvement in tetranuclear clusters at the active site of proteins is expected to modify the interactions with the polypeptide chain involving the latter atoms. Similarly, the larger strain imposed by Se on the active site may induce changes in the electronic structure, as observed with Fd containing two clusters [Gaillard et al. (1987) and references cited therein]. Moreover, the far larger atomic weight of Se compared to S and its very similar chemistry turn it into an unsurpassed label for vibrational studies of Fe–S proteins (Meyer et al., 1986a): the latter property is illustrated by comparison of RR spectra recorded at both $[4Fe\text{-}4X]^{2+}$ and $[4Fe\text{-}4X]^{3+}$ oxidation levels.

The data reported here give compelling evidence that selenium is indeed incorporated into HiPIP in place of inorganic sulfur. The strong similarities between absorption spectra, at both the reduced and oxidized levels (Figures 1 and 2), between EPR data (Figure 3), and between midpoint potentials (Figure 4) for native and Se-reacted HiPIP call for the presence of a [4Fe-4Se] cluster in the latter form. This conclusion is also borne out by the near identity of the RR spectra displayed by reduced Se-containing HiPIP (Figure 5B) and oxidized Se-substituted Fd (Moulis et al., 1984b), for which the presence of $[4Fe\text{-}4Se]^{2+}$ clusters has been unambiguously demonstrated (Moulis & Meyer, 1982). Furthermore, the similar values of the absorption coefficients in the visible range, determined on an iron basis (Figures 1 and 2), and of the purity indexes (Bartsch, 1971; Figures 1 and 2) for native and Se-containing HiPIP agree with the presence of the same amount of chromophore in both forms of the protein. Finally, the observation that native and Se-containing HiPIP titrate similarly with ferricyanide indicates a common number of redox active species and rules out the involvement of clusters of other nuclearity. It is therefore concluded that apoHiPIP specifically refolds around the tetranuclear Se-containing cluster in much the same way as native protein is organized around its active site.

The electronic properties of 4Fe cubane complexes stem from antiferromagnetic coupling between the iron atoms (Cammack et al., 1977). Consequently, the total spin of $[4Fe\text{-}4X]^{2+}$ is zero, and only upon addition, in the case of Fd, or removal, in the case of HiPIP, of one electron does the cluster become paramagnetic, generally with $S = {}^1/_2$. An axial, or slightly rhombic, signal of average g value above 2.0 constitutes the EPR spectra of oxidized HiPIP (Sweeney & Rabinowitz, 1980), except for the Chv protein which displays additional signals in the same field region (Antanaitis & Moss, 1975; Figure 3). Such features do not arise from a mixture of paramagnetic proteins (see Results) and have been found to be induced during the freezing process (Sands, 1979) inherent to the preparation of samples of Fe–S proteins for EPR spectroscopy. A related phenomenon has recently been observed with the nitrogenase Fe protein and has been used to explain (Meyer et al., 1988) the occurrence of two spin species at low temperature (Lindahl et al., 1985). $[4Fe\text{-}4Se]^{3+}$ Chv HiPIP behaves in the same way as its native homologue in displaying a complex EPR spectrum involving the contributions from at least two, and most probably four, sets of g values (Figure 3). Since HiPIP isolated from other sources usually show a simple axial signal (Sweeney & Rabinowitz, 1980), the polypeptide chain appears of foremost importance in creating low-temperature spin-state heterogeneity on tetranuclear Fe–S or Fe–Se clusters. The average g value of the EPR spectrum displayed by Se-HiPIP is higher than that of the native protein, and the corresponding tensor has more split mean values, as already observed with other Se-substituted Fe–S proteins [Gaillard et al. (1986) and references cited therein]. The latter feature might result in part from the stronger strain applied by the polypeptide chain on the larger (Bobrik et al., 1978) [4Fe-4Se] cluster compared to its sulfur homologue.

The midpoint redox potential measured for Se-containing Chv HiPIP (Figure 4) gives the first evidence of a [4Fe-4Se] cluster functioning on the 2+/3+ couple. However, the significant shift of this value observed when Se replaces S* cannot be straightforwardly explained since no precise description of the free energy changes occurring upon electron transfer exists at present for Fe–S proteins. Nevertheless, kinetic data available for HiPIP suggest that a large exposure of the prosthetic group to the environment lowers the energy barrier which has to be overcome prior to electron transfer (Meyer et al., 1983). In this respect, the [4Fe-4Se] cluster of HiPIP, which is larger than the [4Fe-4S] center (Bobrik et al., 1978), might induce a small conformational change around the active site, hence a lower energy barrier to overcome before reaction with redox partners. This suggestion seems at variance with the observation that the redox potential of Cp Fd is insensitive toward the nature of its core chalcogenide (Moulis & Meyer, 1982). However, crystallographic data on *Peptococcus aerogenes* Fd (Adman et al., 1973) reveal a large intrinsic accessibility of the $[4Fe\text{-}4S]^{+/2+}$ clusters to the exterior, and therefore, no significant change in this factor is to be expected from chalcogenide replacement in bacterial low-potential Fd.

The optical properties of both native and Se-substituted forms of Chv HiPIP do not disclose major differences in the electronic transition manifolds, but at both oxidation levels, Se substitution induces bathochromic shifts of some charge transfer absorption bands occurring in the visible range (Figures 1 and 2). It can therefrom be inferred that at least part of the molecular orbitals involved in these transitions have significant X* population and that Se tends to slightly decrease the mean energy difference between occupied X* and unoccupied Fe orbitals, probably by weakening the Fe–X* bonds.

The strong similarities between RR spectra of oxidized Fd (Moulis et al., 1984b) and reduced HiPIP (this work) in terms of the number of bands observed and their distribution over the frequency range confirm that this technique provides an excellent fingerprint for tetranuclear centers in proteins (Meyer et al., 1986a). Such comparisons reveal that the vibrational modes of the $[4Fe\text{-}4X]^{2+}$ complexes, i.e., their local geometry

and their stretching force constants, do not very much depend on their occurrence in HiPIP or Fd. RR spectra of Cp Fd were previously analyzed in D_{2d} symmetry (Moulis et al., 1984c), a framework which has been recently confirmed (Czernuszewicz et al., 1987). The same report (Czernuszewicz et al., 1987) has inferred a smaller cluster distortion from ideal T_d symmetry in the case of HiPIP than for Fd mainly because these authors detected a smaller number of bands in the RR spectra of the former protein. A close inspection of the RR spectra of Figure 5, however, reveals at least nine Raman-active modes (Table I): the 364-cm^{-1} band contains two components (see Results), and the set between 265 and 280 cm^{-1} has reproducibly exhibited a structure of at least two bands. Moreover, a weak but persistent feature is definitely present at 301 cm^{-1} in the spectra of native HiPIP (Figure 5A). Thus, except possibly for a band in the 265–290-cm^{-1} region, RR spectra of oxidized Fd and reduced HiPIP are strictly homologous and should be analyzed in the D_{2d} point group (Moulis et al., 1984c).

The assignments of the cluster fundamental stretching modes performed in D_{2d} symmetry (Moulis et al., 1984c) have recently been reevaluated (Czernuszewicz et al., 1987) by use of extensive IR and RR data on the $[(C_2H_5)_4N]_2[Fe_4S_4(SCH_2C_6H_5)_4]$ analogue in the solid state. Some discrepancies between the two sets of conclusions have mainly focused on the attribution of the Fe–Scys totally symmetric mode. This mode was assigned a 391-cm^{-1} wavenumber for the crystallized model compound, due to the insensitivity of the corresponding Raman band to $^{32\rightarrow34}$S* substitution (Czernuszewicz et al., 1987), whereas our isotopic and polarization data on Cp Fd led us to identify it with the 365-cm^{-1} band (Moulis et al., 1984c). The former authors assigned this mode to a broad band located at 384 cm^{-1} in RR spectra of the synthetic compound in *N*,*N*-dimethylacetamide solution at room temperature and, by analogy, to a 395-cm^{-1} band of the 77 K spectra of Cp Fd, despite its strong isotopic shift (ca. 4 cm^{-1}) upon $^{32\rightarrow34}$S* substitution. This shift value confirms our measurement (5 cm^{-1}; Moulis et al., 1984c) and strongly differs from the 2-cm^{-1} value calculated from normal mode analysis of the model compound (Czernuszewicz et al., 1987). Moreover, the calculated value was obtained by assuming a no less than 40% contribution from bridging modes into this totally symmetric and formally terminal mode (Czernuszewicz et al., 1987). Thus, even a strong vibrational coupling between terminal and bridging bonds does not explain the large isotopic shift measured for the 395-cm^{-1} band. There is hence no compelling reason for reassigning the terminal A_1 mode in RR spectra of Cp Fd, and we maintain our former suggestions which were also consistent with a sizable amount of data on Se-substituted Cp Fd (Moulis et al., 1984c).

As mentioned under Results, the main differences between RR spectra of oxidized Cp Fd and reduced HiPIP lie in the amount of splitting between the vibrational modes attributed to Fe–Scys stretchings; the latter modes occur at 353 and 365 cm^{-1} in [4Fe-4S]$^{2+}$ Cp Fd and at 360 and 363 cm^{-1} in [4Fe-4S]$^{2+}$ HiPIP. For [4Fe-4Se]$^{2+}$ proteins, they stand between 344 and 375 cm^{-1} for Cp Fd and between 348 and 397 cm^{-1} for Chv HiPIP. More generally, all RR spectra reported to date for [4Fe-4S] proteins (Lutz et al., 1983; Johnson et al., 1983; Moulis et al., 1984b,c) exhibit patterns which agree with a core D_{2d} symmetry but disclose variable effects on the stretching modes of the terminal ligands.

The spectra of Figures 5 and 6 give an opportunity to discuss the vibrational properties of the [4Fe-4X] active sites at two distinct redox levels. The spectra of the oxidized 3+ clusters display roughly the same number of Raman-active modes as the spectra of reduced 2+ clusters. It is actually difficult to exactly determine the number of bands between 370 and 435 cm^{-1} in the spectra of Figure 6, but four clearly represents a lower limit. At least 9, and most probably 11, Raman-active stretching modes are thus detected on the entire stretching frequency range in the spectra of oxidized native and Se-substituted HiPIP (Table I). The same data do not easily support a number higher than 11 or 12; i.e., the D_{2d} symmetry point group used to analyze RR spectra of [4Fe-4X]$^{2+}$ in Fd (Moulis et al., 1984c) appears to be relevant in the case of [4Fe-4X]$^{3+}$ clusters in HiPIP as well. This conclusion is not only borne out by the total number of bands detected but also by their wavenumber distribution. It has already been emphasized (see Results) that the bridging modes of the active site at the 3+ oxidation level correspond closely to the same modes at the 2+ level. Therefore, the $Fe_4X^*_4$ moiety most probably retains the same local symmetry in both oxidized and reduced HiPIP. This conclusion does not seem to apply to the part of the active site linking the cluster and the polypeptide.

Fe–Scys stretching modes of HiPIP shift between 10 and 70 cm^{-1} toward higher frequency upon oxidation and most probably undergo significant splittings (Figure 6). It should be mentioned that only four stretching modes are expected from Fe–Scys bonds in the lowest possible symmetry point groups of the cluster (Moulis et al., 1984c) and such a figure is clearly a lower limit for the number of bands observed between 370 and 435 cm^{-1} in spectra of Figure 6 (Table I). Therefore, it might be that, in addition to the splitting induced by a lower symmetry, the terminal modes occur at slightly different frequencies, depending on the various distortions experienced by Fe–Scys bonds. This heterogeneity of the oxidized proteins is reminiscent of that discussed above with EPR spectroscopy. The shift of the Fe–Scys stretching modes to higher wavenumbers indicates that electron removal leads to an increase in the average bond strengths. Assuming that recent theoretical calculations performed on 4Fe active site models of Fd (Noodleman et al., 1985) can be extrapolated to the situation occurring in HiPIP (as suggested by the structural similarities of the clusters in these environments, see above), the HOMO of [4Fe-4S]$^{2+}$ has a pronounced Fe(3d) character: upon oxidation, one electron is removed from this $20a_1$ orbital, i.e., from one specific Fe–Fe subdimer, and the highest occupied orbitals within the more oxidized half of the active site then become of mainly S(3p) character ($13b_2$ or $14b_1$). The more reduced half retains the extra electron of the mixed-valence Fe–Fe pair in $20a_1$ (Noodleman et al., 1985). The description of the oxidized HiPIP cluster as composed of two distinct Fe–Fe pairs stems from the features of Mössbauer spectra (Middleton et al., 1980; Papaefthymiou et al., 1986) and is consistent with all the parameters derived from them (Noodleman, 1988). Electron removal not only affects HOMO and LUMO but is also expected to induce a large electronic relaxation on the whole structure. Molecular orbitals of mainly Scys(3p) character will participate more actively to this phenomenon than those involving X* since, due to the greater polarizability of the *S*-cysteine ligands compared to μ_3-X, they respond more efficiently to the relative electron deficiency created by oxidation on one Fe–Fe pair (Noodleman and Case, work in progress). Specific increases in the frequencies of RR modes in adrenodoxin upon oxidation have recently been attributed to weaker H-bonding (Mino et al., 1987). The same type of explanation might be proposed here for HiPIP, but X-ray crystallographic data (Carter, 1977) reveal that H-bond lengthening upon oxidation applies equally

to NH···S distances involving both Scys and S*. Hydrogen bonding is therefore unlikely to account for the specific effect observed on terminal bonds when Figures 5 and 6 are compared.

The marked splitting of the Fe–Scys stretching modes in the spectra of oxidized HiPIP (Figure 6) denotes a less symmetrical distribution of force constants on the corresponding bonds than occurs in the reduced species. This effect is most probably related to a geometric distortion of the terminal bonds which breaks their near equivalence observed at the reduced level (see above). A consequence of the asymmetry induced by oxidation on the terminal bonds may be looked for in the changes affecting the hydrogen bond network surrounding the active site: the NH···Scys distances increase by 0.4 and 0.2 Å for bonds involving Cys_{63} and Cys_{77}, respectively, while changes affecting the two hydrogen bonds on Cys_{46} can hardly be detected (Carter, 1977). For this description to be totally consistent with RR data, one has to assume that the vibrational coupling of terminal and bridging modes is weak at both oxidation levels. No definitive information yet exists on this point, but S/Se substitution provides some indication; the terminal modes occur at about the same (within ca. 10 cm^{-1}) frequencies with either S* or Se* both in Fd (Moulis et al., 1984c) and HiPIP (this work) despite the large reduced mass difference between Fe_4S_4 and Fe_4Se_4. The simplest explanation for such a behavior is indeed that of a weak coupling between the terminal and bridging modes.

In summary, we propose the following interpretation of RR spectra of oxidized HiPIP. The loss of one electron in a $20a_1$, mainly Fe–Fe, orbital upon oxidation induces electron flow from Fe–Scys antibonding or nonbonding orbitals (Noodleman et al., 1985; Aizman & Case, 1982; Noodleman & Baerends, 1984) to screen the resulting positive hole. A significant decrease in electron density over the terminal bonds and a strengthening of these bonds occur. Such rearrangement does not have to be uniform over all cysteine groups as indicated by the large splitting of the Fe–Scys stretching modes (Figure 6) and by the variable lengthenings of the hydrogen bonds involving Scys atoms (Carter, 1977). From a functional perspective, a subset of one or two Fe–Scys bonds might be a privileged electron exchanger with the exterior of the molecule, thus playing a primary role in the redox process. Additional RR data and further calculations on [4Fe-4X] proteins are expected to shed some light on the soundness of this hypothesis.

In addition to previous work on bacterial Fd [Moulis et al., 1984c; Gaillard et al. (1987) and references cited therein], the availability of $[4Fe\text{-}4Se]^{2+/3+}$ HiPIP has given insight into the role played by the various atoms of the 4Fe structure in proteins. As with *B. stearothermophilus* Fd (Gaillard et al., 1986), the electronic structure of the cluster is only marginally affected by the core chalcogenide substitution, and the protein retains its redox properties. However, the vibrational modes of the active site display a high sensitivity toward this replacement and allow separation of the contributions from the bridging and the terminal bonds. Moreover, the molecular rearrangement occurring during the redox process can be analyzed through the obtention of RR spectra at two different oxidation levels with HiPIP: this offers new perspective for investigation of the presently unknown mechanism of electron transfer with Fe–S proteins, by use of time-resolved Raman spectroscopy for instance.

ACKNOWLEDGMENTS

We thank Professor Michael A. Cusanovich for his kind gift of Chv HiPIP and for valuable comments. Careful reading of the manuscript, precious advice, and continuous encouragement from Dr. Jacques Meyer are gratefully acknowledged.

REFERENCES

Adman, E. T., Sieker, L. C., & Jensen, L. H. (1973) *J. Biol. Chem. 248*, 3987–3996.

Aizman, A., & Case, D. A. (1982) *J. Am. Chem. Soc. 104*, 3269–3279.

Antanaitis, B. C., & Moss, T. H. (1975) *Biochim. Biophys. Acta 405*, 262–279.

Auric, P., Gaillard, J., Meyer, J., & Moulis, J.-M. (1987) *Biochem. J. 242*, 525–530.

Bartsch, R. G. (1971) *Methods Enzymol. 23A*, 644–649.

Bartsch, R. G. (1978) *Methods Enzymol. 53B*, 329–340.

Blair, D., & Diehl, H. (1961) *Talanta 7*, 163–174.

Bobrik, M. A., Laskowski, E. J., Johnson, R. W., Gillum, W. O., Berg, J. M., Hodgson, K. O., & Holm, R. H. (1978) *Inorg. Chem. 17*, 1402–1409.

Cammack, R., Dickson, D. P. E., & Johnson, C. E. (1977) in *Iron-Sulfur Proteins* (Lovenberg, W., Ed.) Vol. III, pp 283–330, Academic, New York.

Carter, C. W., Jr. (1977) in *Iron-Sulfur Proteins* (Lovenberg, W., Ed.) Vol. III, pp 157–206, Academic, New York.

Carter, C. W., Jr., Kraut, J., Freer, S. T., Alden, R. A., Sieker, L. C., Adman, E. T., & Jensen, L. H. (1972) *Proc. Natl. Acad. Sci. U.S.A. 69*, 3526–3529.

Carter, C. W., Jr., Kraut, J., Freer, S. T., & Alden, R. A. (1974) *J. Biol. Chem. 249*, 6339–6346.

Czernuszewicz, R. S., Macor, K. A., Johnson, M. K., Gewirth, A., & Spiro, T. G. (1987) *J. Am. Chem. Soc. 109*, 7178–7187.

Gaillard, J., Moulis, J.-M., Auric, P., & Meyer, J. (1986) *Biochemistry 25*, 464–468.

Gaillard, J., Moulis, J.-M., & Meyer, J. (1987) *Inorg. Chem. 26*, 320–324.

Johnson, M. K., Thomson, A. J., Robinson, A. E., Rao, K. K., & Hall, D. O. (1981) *Biochim. Biophys. Acta 667*, 433–451.

Johnson, M. K., Czernuszewicz, R. S., Spiro, T. G., Ramsay, R. R., & Singer, T. P. (1983) *J. Biol. Chem. 258*, 12771–12774.

Lindahl, P. A., Day, E. P., Kent, T. A., Orme-Johnson, W. H., & Münck, E. (1985) *J. Biol. Chem. 260*, 11160–11173.

Lutz, M. (1977) *Biochim. Biophys. Acta 460*, 408–430.

Lutz, M., Moulis, J.-M., & Meyer, J. (1983) *FEBS Lett. 163*, 212–215.

Meyer, J., & Moulis, J.-M. (1981) *Biochem. Biophys. Res. Commun. 103*, 667–673.

Meyer, J., Moulis, J.-M., & Lutz, M. (1986a) in *Frontiers in Bioinorganic Chemistry* (Xavier, A. V., Ed.) pp 537–546, VCH Verlag, Weinheim.

Meyer, J., Moulis, J.-M., & Lutz, M. (1986b) *Biochim. Biophys. Acta 871*, 243–249.

Meyer, J., Moulis, J.-M., & Lutz, M. (1986c) *Biochim. Biophys. Acta 873*, 108–118.

Meyer, J., Gaillard, J., & Moulis, J.-M. (1988) *Biochemistry 27*, 6150–6156.

Meyer, T. E., Przysiecki, C. T., Watkins, J. A., Bhattacharyya, A., Simondsen, R. P., Cusanovich, M. A., & Tollin, G. (1983) *Proc. Natl. Acad. Sci. U.S.A. 80*, 6740–6744.

Middleton, P., Dickson, D. P. E., Johnson, C. E., & Rush, J. D. (1980) *Eur. J. Biochem. 104*, 289–296.

Mino, Y., Loehr, T. M., Wada, K., Matsubara, H., & Sanders-Loehr, J. (1987) *Biochemistry 26*, 8059–8065.

Mizrahi, I. A., Meyer, T. E., & Cusanovich, M. A. (1980) *Biochemistry 19*, 4727–4733.

Moulis, J.-M., & Meyer, J. (1982) *Biochemistry 21*, 4762–4771.
Moulis, J.-M., Auric, P., Gaillard, J., & Meyer, J. (1984a) *J. Biol. Chem. 259*, 11396–11402.
Moulis, J.-M., Meyer, J., & Lutz, M. (1984b) *Biochem. J. 219*, 829–832.
Moulis, J.-M., Meyer, J., & Lutz, M. (1984c) *Biochemistry 23*, 6605–6613.
Noodleman, L. (1988) *Inorg. Chem.* (in press).
Noodleman, L., & Baerends, E. J. (1984) *J. Am. Chem. Soc. 106*, 2316–2327.
Noodleman, L., Norman, J. G., Jr., Osborne, J. H., Aizman, A., & Case, D. A. (1985) *J. Am. Chem. Soc. 107*, 3418–3426.
Papaefthymiou, V., Millar, M. M., & Münck, E. (1986) *Inorg. Chem. 25*, 3010–3014.
Sands, R. H. (1979) in *Multiple Electron Resonance Spectroscopy* (Dorio, M. M., & Freed, J. H., Eds.) pp 331–374, Plenum, New York.
Spiro, T. G., Hare, J., Yachandra, V., Gewirth, A., Johnson, M. K., & Remsen, E. (1982) in *Iron-Sulfur Proteins* (Spiro, T. G., Ed.) pp 407–423, Wiley-Interscience, New York.
Sweeney, W. V., & Rabinowitz, J. C. (1980) *Annu. Rev. Biochem. 49*, 139–161.

Effect of Solvent Viscosity on the Heme-Pocket Dynamics of Photolyzed (Carbonmonoxy)hemoglobin†

E. W. Findsen,‡ J. M. Friedman,§ and M. R. Ondrias*,‡

Department of Chemistry, University of New Mexico, Albuquerque, New Mexico 87131, and AT&T Bell Laboratories, Murray Hill, New Jersey 07974

Received March 11, 1988; Revised Manuscript Received July 21, 1988

ABSTRACT: The heme-pocket dynamics subsequent to carbon monoxide photolysis from human hemoglobin have been monitored as a function of glycerol–water solvent composition with time-resolved resonance Raman spectroscopy. Prompt (geminate) ligand recombination rates and the transient heme-pocket geometry established within 10 ns after photolysis appear to be largely independent of solvent composition. The rate of relaxation of the transient geometry to an equilibrium deoxy configuration is, however, quite sensitive to solvent composition. These observations suggest that the former processes result from local, internal motions of the protein, while the relaxation dynamics of the proximal heme pocket are predicated upon more global protein motions that are dependent upon solvent viscosity.

During the past 2 decades, an increasing number of experimental and theoretical studies [for review, see Gurd and Rothgeb (1979), Debrunner and Frauenfelder (1982), Karplus and McCammon (1983), and Rousseau and Friedman (1988)] have demonstrated that structural dynamics play a pivotal role in the functional processes of metalloproteins. The complexity of proteins allows for many levels of structural dynamics, each having the potential to influence net protein function. These can range from local fluctuations of atoms or side chains about equilibrium positions to concerted motions of entire domains as the protein structure changes between equilibrium conformations. Both fluctuational dynamics and transitions between equilibrium conformations (either local or global) depend upon environmental factors. However, the various levels of protein dynamics may exhibit different responses to solvent viscosity. Motions at the protein surface or concerted motions of protein domains would be expected to be quite sensitive to solution properties, whereas local dynamics of the protein interior are influenced by viscosity only to the extent that they are coupled to more global dynamics. This study examines the extent to which protein–solvent interactions directly affect the ligand binding dynamics at the heme active site of hemoglobin.

The kinetics of ligand (CO, O_2) binding to hemoglobin (Hb) and myoglobin (Mb) have been well characterized by transient absorption measurements (Morris & Gibson, 1984; Gibson et al., 1986; Campbell et al., 1985; Hasinoff & Chishti, 1983, 1982; Hasinoff, 1981; Beece et al., 1980; Doster et al., 1982; Austin et al., 1975). In particular, Frauenfelder and co-workers have used this technique to great advantage. Their analyses of ligand rebinding subsequent to photolysis over a wide range of temperatures and solution conditions have revealed a power-law behavior for religation which can be described as motion of the ligand over a series of potential energy barriers each having a distribution of heights that is dependent upon the conformational properties of the protein. Several transient absorption studies have demonstrated the dependence of ligand recombination rates upon solvent viscosity (Hasinoff & Chishti, 1982, 1980; Hasinoff, 1981). A more detailed analysis of MbCO by Frauenfelder and co-workers (Beece et al., 1980) revealed that all except the innermost potential barriers encountered by the migrating ligand were viscosity dependent. This clearly implies that protein–solvent dynamics can regulate the dynamics of the interior protein motions.

The time-resolved resonance Raman techniques employed in this study provide data that complement the transient absorption studies. Resonance Raman scattering selectively interrogates the heme active site of hemoglobin. Moreover, the heme vibrational spectrum can be interpreted to provide specific molecular details about the active site (Spiro, 1983; Rousseau & Ondrias, 1983). Recently, time-resolved reso-

† This work was performed at the University of New Mexico and was supported by the NSF (DMB8604435).
‡ University of New Mexico.
§ AT&T Bell Laboratories.

0006-2960/88/0427-8719$01.50/0